Hindawi
International Journal of Antennas and Propagation
Volume 2023, Article ID 1566430, 23 pages
https://doi.org/10.1155/2023/1566430

Research Article

Performance Analysis of MIMO Antenna Design with High Isolation Techniques for 5 G Wireless Systems

Suverna Sengar,[1] Praveen Kumar Malik,[1] Puneet Chandra Srivastava,[2] Kiran Srivastava,[3] and Anita Gehlot[4]

[1]*School of Computer Science and Engineering, Lovely Professional University, Phagwara, Punjab, India*
[2]*Rajkumar Goel Institute of Technology, Ghaziabad, India*
[3]*Galgotias College of Engineering and Technology, Greater Noida, UP, India*
[4]*Division of Research and Innovation, Uttaranchal University, Dehradun, Uttrakhand, India*

Correspondence should be addressed to Praveen Kumar Malik; pkmalikmeerut@gmail.com

Received 22 July 2023; Revised 30 October 2023; Accepted 8 November 2023; Published 29 November 2023

Academic Editor: Sandeep Kumar Palaniswamy

This paper investigates different approaches for achieving isolation in a MIMO antenna design. It provides an in-depth comparison of these techniques, analyzing their advantages and disadvantages. The challenges of obtaining sufficient isolation in modern MIMO antenna design are discussed, and various isolation methods developed for the MIMO design are examined. The study introduces a compact 28 GHz 4-port MIMO antenna design, which is placed on a Rogers RT/Duroid 5880 substrate. The design includes a rectangular patch with semicircles at the ends and dual slots etched from it. A partial ground plane is integrated into the antenna to achieve an operating frequency range from 22 to 29 GHz, centered at 24 GHz. To reduce mutual coupling between elements, four elements are arranged orthogonally and four stubs are added at a specific frequency band to enhance isolation. The ground plane also incorporates a defected ground structure (DGS) to improve gain. To optimize the antenna's bandwidth, a ground cut technique is used, resulting in a 0.7 GHz bandwidth enhancement at the cost of some isolation. The antenna operates in the range of 22.5– 29.1 GHz, with a peak gain of 6.39 dBi. Each technique is compared based on parameters such as *S*-parameters (return loss or reflection coefficient), voltage standing wave ratio (VSWR), isolation level, and peak gain. Simulated results are shown for each of the techniques to compare their performance by using Ansys HFSS simulations which confirm that the designed antenna meets the target band requirements and could be used in 5 G communications.

1. Introduction

Recent advancements in affordable millimeter-wave (mm-W) RF-integrated circuits and devices have made it possible to use MIMO techniques at frequencies up to 24 GHz. This feature proves extremely advantageous in catering to the increased data transfer requirements of the upcoming 5 G wireless cellular networks and advancements in the Internet of Things (IoT) [1–3]. The International Telecommunication Union (ITU) has set a requirement of around 20 Gbps for the channel capacity of 5 G networks. To meet this growing demand for data rate, it is crucial to combine the wide bandwidth available in mm-W bands with the improved channel throughput achieved through MIMO techniques. This combination allows for higher data rates and improved performance in future wireless networks [4, 5].

The performance of MIMO antennas and the propagation channel at the 24 GHz band is significantly affected by mutual coupling (MC). The degradation of the array radiation pattern, side lobe level, gain, impedance matching, and channel capacity is affected by this impact [6–8]. In certain scenarios, it is crucial to maintain a minimum mutual coupling level of −25 dB in certain applications. In MIMO systems, it is necessary to have high isolation levels between radiating elements in order to ensure a low envelope correlation coefficient [9]. Therefore, it is vital to consider the

isolation between antenna elements during the design phase of MIMO systems to successfully implement antenna diversity schemes.

Previous research has found that the interaction between antennas, known as mutual coupling, can negatively impact the correlation and efficiency of diversity antenna solutions [10, 11]. Therefore, minimizing the correlation between antenna ports is essential for achieving high diversity gain. The emergence of 5 G has brought about massive MIMO technology, which has shown great potential in increasing channel capacity compared to traditional MIMO systems in real-world settings [12]. However, compact MIMO antennas are preferred for mobile terminals and base stations. Unfortunately, the close proximity of these antennas makes electromagnetic mutual coupling inevitable, leading to changes in input impedance, reflection coefficients, and radiation patterns of the array elements. As a result, it is incredibly important to create methods aimed at reducing the impacts of mutual coupling in the antenna design. Numerous strategies have been developed to tackle this problem, such as polarization diversity, the use of defected ground structure (DGS), electromagnetic band-gap (EBG) techniques, and the integration of parasitic elements amidst antennas. Additionally, various other methods are employed to counter the coupling in MIMO antennas for ultra-wideband (UWB) applications [13]. These methods include spatial, pattern, polarization, and decoupling structures, as well as the use of metamaterials. EBG structures are integrated to eliminate surface wave occurrence, leading to a reduction in the in-phase reflection coefficient and associated coupling. Complimentary split ring resonators (CSRRs) are utilized for their ability to filter and enhance isolation, employing a series of extended metal strips [14]. In further research, different diversity techniques such as spatial, polarization, and pattern models, as well as methods for reducing mutual coupling such as parasitic approaches, neutralization lines, slot/slit etching, meta-materials, and coupling/decoupling networks, are investigated [15, 16].

As shown in Table 1, many other researchers improved the isolation of MIMO antenna. But they provided the maximum isolation of 25 dB, but here, in the proposed MIMO antenna design, we achieved improved isolation near about 29 dB.

This paper explains the design process of a miniaturized quad-port MIMO antenna with a board size of $(40 \times 40)\text{mm}^2$ and placed on Rogers RT/Duroid 5880 substrate is utilized, featuring a 0.8 mm thickness, a dielectric constant ($\varepsilon_r = 2.2$), and loss tangent ($\delta = 0.0009$). Isolation techniques such as modified ground structure (MGS), decoupling (parasitic element) structure, and defected ground structure (DGS) were applied, respectively. Furthermore, parameters such as VSWR, *S*-parameters, peak gain, and radiation efficiency were simulated with the software Ansys HFSS. The results showed that the decoupling technique achieved the highest isolation in the entire band of frequency range among the applied techniques. Thus, the quad-port MIMO antenna design would benefit the most from the decoupling isolation technique.

The proposed antenna significantly advances the field of MIMO antenna design for 5 G wireless systems by introducing innovative designs, demonstrating improved isolation techniques, and providing concrete performance analysis. It helps to address the growing demand for high-performance antennas in the rapidly evolving of 5 G wireless communication.

The paper is organized as follows. Introduction and comparative studies are discussed in Section 1. Antenna geometry and design are discussed in Section 2. Different isolation techniques are covered with the effects of varying resonant frequencies and antenna characteristics on the outcomes of the research are described in the Section 3 and it also presents the comparison of the proposed design with different isolation techniques. Finally, Section 4 concludes the study.

2. Antenna Geometry and Design

The antenna design for 5 G wireless applications should have multiple-input multiple-output (MIMO) capabilities. The antenna should be able to support an ultra-wideband frequency range from 20 GHz to 30 GHz for MIMO and 5 G wireless applications. The antenna should have high directivity and high gain in order to maximize connectivity between wireless devices. The antenna should also have wide beam width coverage and low side lobe levels in order to reduce interference and crosstalk in an area with a high density of users. To further enhance the signal and data transmission capacity of the antenna, polarization diversity should be considered. The impedance should be matched with 50 ohms with the lowest possible VSWR to ensure efficient data transmission. The design should also incorporate high isolation between each antenna element to avoid any interference and crosstalk [30–32].

An elliptical design antenna has advantages over rectangular- and circular-shaped antennas in certain situations. Here are some reasons why an elliptical design may be preferred:

(1) Compared to rectangular and circular antennas, elliptical antennas can achieve wider bandwidths. This is particularly useful in applications such as ultra-wideband (UWB) communication systems, where a broad frequency range is needed for high data rates and spectral efficiency.

(2) The elliptical shape allows for better impedance matching across a wide frequency range than rectangular and circular antennas. This leads to fewer signal reflections and improved power transfer efficiency.

(3) Circular antennas often have more cross-polarization, which can cause increased interference and signal deterioration. In contrast, elliptical antennas tend to have better cross-polarization characteristics, resulting in improved signal quality and reduced interference in polarization-sensitive applications.

The antenna's impedance characteristics are determined using the following equation:

$$Z_0 = \frac{Z_{01}}{\sqrt{\varepsilon_e}}, \tag{1}$$

Table 1: State-of-the-art comparison with isolation techniques.

Ref. no	No. of elements	Size (mm^3)	Substrate	Operating frequency (GHz)	Gain (dBi)	Isolation (dB)	Isolation technique	Applications
[17]	4	$25 \times 12 \times 0.381$	Roger RT/Duroid 5880	1.8–2.6 25–40	7.2	≥17	Tapered slot	Integrated 5 G/4 G in the same structure, mm-wave
[18]	4	Diameter = 30.6 mm with 2 mm height	FR4	3.3 to 4.2	6.21	>9.7	—	5 G applications
[19]	2	$48 \times 35 \times 1.6$	FR4-epoxy	2.1–18	2–8	>20	Metamaterials (SRR)	UWB applications
[20]	4	$60 \times 60 \times 1.6$	FR4	3–16.2	10.55	>17.5	EGB	Modern wireless communication systems
[10]	2	$50 \times 30 \times 1.6$	FR4	2.5–14.5	7.4	>20	*F*-shaped stubs	UWB applications
[21]	4	$80 \times 80 \times 1.6$	FR4	2.1–20	5.8	>25	*H*- and *U*-slots	WiMAX and military/radar applications
[22]	4	$48 \times 52 \times 1.6$	FR4	2.7–11	3.5	>20	Asymmetric coplanar strip (ACS) feed	WiMAX applications
[23]	4	$18 \times 16 \times 1.57$	RT/Duroid 5870	5.6–6.05	7.98	>24	DNG metamaterial superstrate	WLAN applications
[24]	4	$36.2 \times 36.2 \times 5$	Rogers RT 4003	36.6–39.5	10	>25	FSS	5 G communications
[25]	4	$24 \times 20 \times 1.85$	Transparent conductive sheet AgHT-8	24.10–27.18; 33–44.13	3	>16	Undivided ground plane	*n* low profile smart devices at mm-wave 5 G applications
[26]	4	$80 \times 80 \times 1.57$	Rogers 5880	23–40	12	>20	—	5 G·mm-wave applications
[27]	4	$30 \times 35 \times 0.76$	Rogers R04350B	25.5–29.6	8.3	>10	Zig-zag shaped DGS	5 G·mm-wave applications
[28]	4	—	Rogers RT/Duroid 5880	22.5–32	8.2–9.6	>20	Substrate integrated waveguide (SIW)	Multichannel millimeter-wave transceivers
[29]	2×2	$41.3 \times 46 \times 0.508$	Rogers RT/Duroid 5880	27.5–31.44	13.1	>23	*U*-slots	mm-wave applications

where the microstrip line's impedance in free space is given by the following equation:

$$Z_{01} = Z_0 \left| (\varepsilon r = 1) = 60 \ln \left[\frac{F_1 h}{w} + \sqrt{1 + \left(\frac{2h}{w} \right)^2} \right], \right. \quad (2)$$

$$F_1 = 6 + (2\pi - 6)\exp\left\{ -(30.66h/\omega)^{0.7528} \right\}.$$

The effective width and height of the antenna can be computed using the following expressions (3), (4), and (7):

$$W = w + \frac{t}{\pi} \left[\ln\left(\frac{2h}{t} \right) + 1 \right], \quad (3)$$

Here, $H = h - 2t$.

For $W/H < 1$,

$$\varepsilon_{\text{eff}} = \frac{\varepsilon r + 1}{2} + \frac{\varepsilon r - 1}{2} \left[\frac{1}{\sqrt{1 + 12\,(H/W)}} + 0.04\left(1 - \frac{W}{H} \right) 2 \right],$$

$$Z_0 = \frac{60}{\sqrt{\varepsilon_{\text{eff}}}} \ln\left(\frac{8H}{W} + \frac{W}{4H} \right) \Omega. \quad (4)$$

Also,

$$\lambda = \frac{c}{f\sqrt{\varepsilon_{\text{eff}}}}, \quad \theta = \frac{2\pi}{\lambda}. \quad (5)$$

For $W/H \geq 1$,

$$\varepsilon_{\text{eff}} = \frac{\varepsilon_{r+1}}{2} + \frac{\epsilon_{r-1}}{\sqrt[2]{1 + 12\,(H/W)}}. \quad (6)$$

The equation that describes the relation between characteristic impedance Z_0^{MPA} and the width of a microstrip line is quite straightforward [33–35].

$$Z_0^{\text{MPA}} = \frac{120\pi}{\sqrt{\varepsilon_r \left[(w/h) + 1.393 + 0.667 \ln\left((w/h) + 1.444 \right) \right]}}. \quad (7)$$

The width of the microstrip line is represented by variable w, which is around 0.55 mm, and h is the height, which is 0.8 mm, and $Z_0^{\text{MPAfeed}} = 50\Omega$.

Elliptical geometry is as follows:

$$e = \sqrt{1 - \left(\frac{b}{a} \right)^2}. \quad (8)$$

In an elliptical patch, the major axis is represented by "a," the minor axis is represented by "b," and the eccentricity is represented by "e."

The equation of resonance frequency calculation for dual band elliptical slots is as follows:

$$f_{11}^{e,0} = \frac{15}{\pi e a_{\text{eff}}} \sqrt{\frac{Q_{11}^{e,0}}{\varepsilon_r}} \text{GHz}, \quad (9)$$

$$a_{\text{eff}} = a\sqrt{\left[1 + \frac{2h}{\pi \varepsilon_r a} \left\{ \ln\left(\frac{a}{2h} \right) + \left(1.41\varepsilon_r + 1.77 \right) + \frac{h}{a} \left(0.268\varepsilon_r + 1.65 \right) \right\} \right]}, \quad (9a)$$

$$Q_{11}^e = -0.0049e + 3.788e^2 - 0.7228e^3 + 2.2314e^4, \quad (9b)$$

$$Q_{11}^0 = -0.0063e + 3.832e^2 - 1.1351e^3 + 5.2229e^4. \quad (9c)$$

The wavelength is determined using the following equation:

$$\lambda_g = \frac{c}{f\sqrt{\varepsilon_r}}. \quad (10)$$

To obtain the diameter of the elliptical patch for both low cut-off frequency and high cut-off frequency, the following expression is used:

$$f_L = \frac{72}{L + r + h}, \quad (11)$$

where L represents the diameter of the radiator, h is the substrate thickness, and r can be calculated using the following equation:

$$r = \frac{L}{2\pi}. \quad (12)$$

Considering a substrate with a dielectric permittivity of 2.2 and a thickness of 0.8 mm and equations (1)–(12) [32–35].

3. Isolation Techniques

There are lots of isolation techniques but here we are going to show only few of them and we are going to compare their simulated results, and based on the results, we will explain which isolation technique provided the best results for this proposed MIMO antenna.

3.1. Self-Isolation Techniques. It is often used to control the antenna's radiation pattern and impedance matching. The design parameters for self-isolation, such as the width and placement of the ground slots, depend on the desired electrical performance. Simulations that use tools, such as electromagnetic simulation software HFSS, can help optimize these parameters. In this technique, the spacing between the radiating elements has been enlarged from one quarter ($\lambda/4$) of the wavelength to half of the wavelength ($\lambda/2$). This increase in distance results in improved isolation between the radiating elements.

The MIMO antenna structure displayed in Figure 1 has been simulated and modeled using HFSS. RT/Duroid-5880 substrate with low dielectric losses was selected to construct the antenna. This particular substrate has a dielectric constant of 2.2, a loss tangent of 0.0009, and a thickness of 0.8 mm. The dimensions of the substrate are $L_s \times W_s\,\text{mm}^2$. The four antenna elements, namely, Ant-1–Ant-4, are printed on the four sides of the substrate. The microstrip feeding lines are placed on the top layer of the substrate, while a portion of the ground plane on the bottom layer is etched away.

In Figure 2, the dimensions of the self-isolated MIMO antenna are shown. All dimensions are defined in mm with respect to parameters in Table 2.

Figure 3 displays the complete simulated outcomes of a self-isolated MIMO antenna. Figure 3(a) illustrates the return loss ($S11$), with the highest value being recorded at −12.88, occurring at a frequency of 23.7 GHz. This is accompanied by an ultra-wideband of 7.8 GHz. Figure 3(b) showcases the VSWR, which remains consistently below 2. Additionally, the antenna demonstrates an overall gain surpassing 3.7 dB or 5.85 dBi across the entire frequency range, while achieving an isolation level greater than −23 dB. A sudden decay in gain at the middle band could be attributed to a combination of multiple factors such as frequency resonance and bandwidth and antenna design and its geometry that might necessitate adjustments to the antenna design to ensure consistent performance across the entire frequency range. Antennas are designed to operate efficiently within a specific frequency range, and their gain decreases rapidly as they move away from the resonant frequency region. This is a fundamental characteristic of antennas and is crucial to consider when designing and using them for specific applications.

3.2. Modification of the Partially Ground Structure. In this method, we made alterations to the ground and the two rectangular slots in different locations and orientations, while keeping the same dimensions. By doing so, we incorporated open-source ground cuts that enhance the antenna bandwidth and gain. The antenna design uses the same substrate with the top layer for microstrip feeding lines, while a portion of the modified ground plane is etched on the bottom layer. The modified ground structure antenna design is depicted in Figure 4, which shows both the top and bottom views. The dimensions of the MIMO antenna with the modified ground structure (MGS) are illustrated in Figure 5. All measurements are specified in millimeters, as detailed in Table 3.

The data presented in Figure 6 illustrate the outcomes of the MIMO antenna with a modified ground structure. Figure 6(a) displays the return loss ($S11$), showcasing a maximum return loss of −14 at a frequency of 21.5 GHz with an extensive ultra-wideband of 8.8 GHz. Figure 6(b) demonstrates the VSWR, which remains below 2. Furthermore, the antenna exhibits an overall gain exceeding 3.71 dB or 5.86 dBi throughout the entire frequency band, accompanied by an isolation level exceeding −23 dB. This technique significantly enhances the bandwidth, implying that modifying the ground structure leads to an enhanced bandwidth.

3.3. Decoupling Structure. The decoupling structure is designed to reduce mutual coupling between antenna elements in the MIMO array. Techniques such as electromagnetic band gap (EBG) structures or slotted ground planes can be employed. The design of decoupling structures involves tuning the dimensions and positions of the elements to minimize mutual coupling. An antenna configuration employing a quad-port MIMO structure has been created and simulated using the Ansys HFSS software. The design is implemented on an RT/Duroid-5880 substrate, which was selected for its minimal dielectric losses. This substrate possesses a dielectric constant of 2.2, a loss tangent of 0.0009, and a thickness of 0.8 mm, with dimensions of $(L \times W)\,\text{mm}^2$. Each of the four antenna elements (Ant-1–Ant-4) are printed on one of the four sides of the substrate. The top layer of the substrate is used to place the microstrip feeding lines with introducing the X-shaped decoupling structure on the radiating patch, while part of the ground plane at the bottom layer is etched. Here, Figure 7 shows the top and bottom views with decoupling structure antenna design. Figure 8 shows the dimensions of the MIMO antenna by introducing the X-shaped decoupling structure. All dimensions are defined in mm with respect to parameters in Table 4.

Figure 9 shows all simulated results of MIMO antenna with decoupling structure (introducing the X-shaped wall between the radiating elements). Figure 9(a) shows return loss ($S11$); the maximum return loss is −14.38 at 24 GHz frequency with a wideband of 6.6 GHz. Figure 9(b) shows the VSWR which is less than 2, and the overall gain of the antenna within the entire band is greater than 2 dB or greater than 4.15 dBi and isolation is increased from −23 dB to −27.63 dB. In this technique, the bandwidth is little bit decreased but isolation is improved; so, this technique is good for improving the isolation.

3.4. Defected Ground Structure. DGS can be employed to control the radiation properties of the antenna and reduce unwanted radiation in certain directions. The quad-port antenna system with MIMO configuration and isolation method was created and tested using the Ansys HFSS software. The design was implemented on RT/Duroid-5880 substrate, which was chosen for its minimal dielectric losses. The substrate has specific characteristics, including a dielectric constant of 2.2, a loss tangent of 0.0009, a thickness of 0.8 mm, and dimensions of $L \times W\,\text{mm}^2$. Each of the four

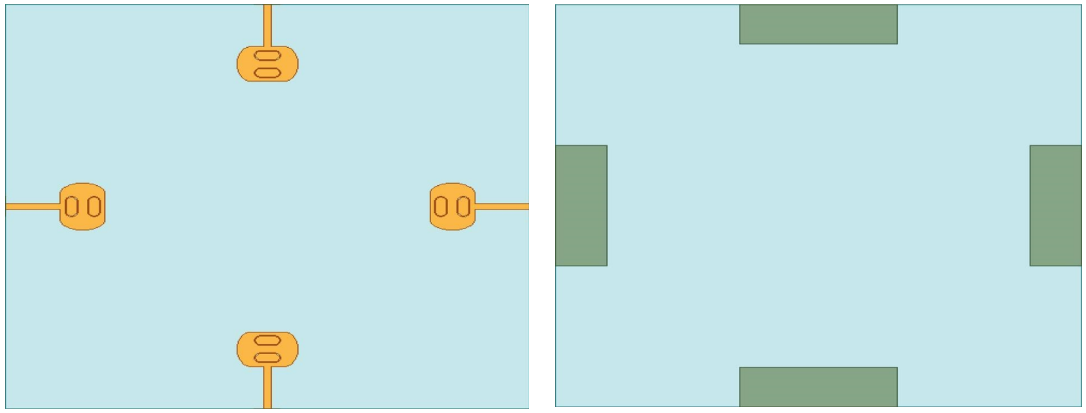

Figure 1: Self-isolated MIMO antenna design: (a) top view and (b) bottom view.

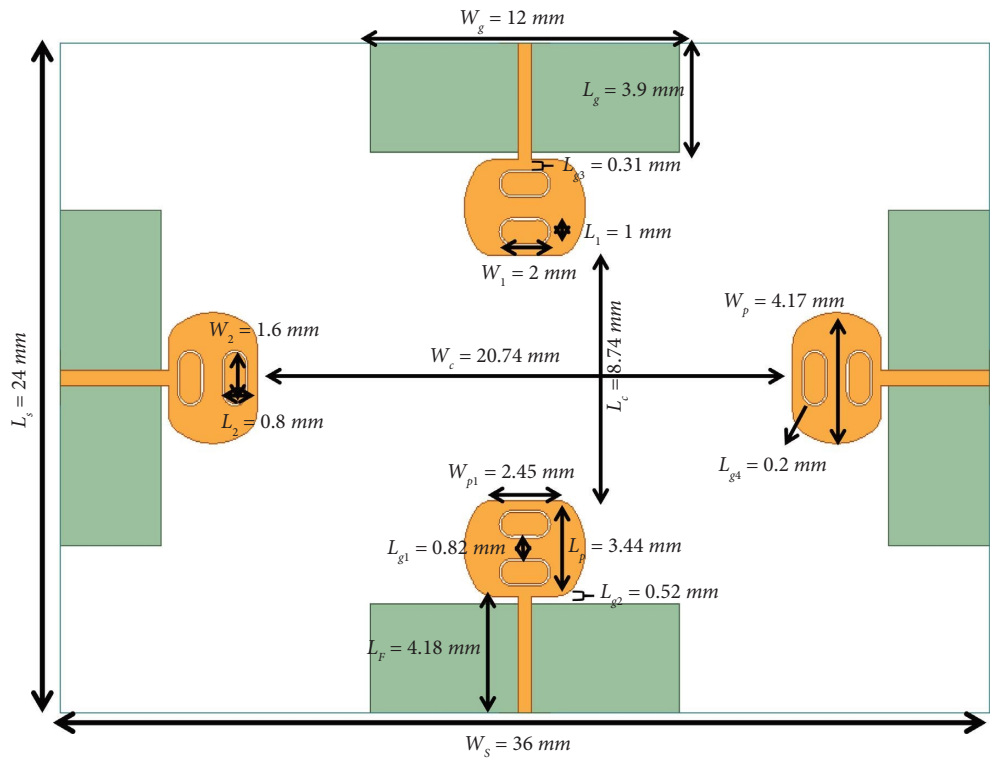

Figure 2: Dimensions of the self-isolated MIMO antenna.

antenna elements (Ant-1–Ant-4) are positioned on different sides of the substrate. The top layer of the substrate is used to place the microstrip feeding lines, while a part of the defected ground (introducing square mesh type-defected ground structure) plane at the bottom layer is etched. Here, Figure 10 shows the top and bottom views of the defected ground structure antenna design. Figure 11 shows the dimensions of the MIMO antenna with defected ground structure (DGS). All dimensions are defined in mm values with respect to parameters in Table 5.

Figure 12 displays the simulated outcomes of a MIMO antenna integrated with a defected ground structure. The initial graph in Figure 12 presents the return loss ($S11$), with the highest return loss of −14.73 observed at a frequency of 25.8 GHz. This frequency holds an ultra-wideband of 7.6 GHz. The following graph exhibits the voltage standing wave ratio (VSWR), which remains below 2. Throughout the entire bandwidth, the antenna showcases an overall gain higher than 4.14 dB or 6.29 dBi, accompanied by isolation exceeding −24 dB.

Table 2: Optimal values of the self-isolated MIMO antenna dimensions (all in mm).

Parameters	Values (mm)
W_S	40
L_S	40
H_S	0.8
W_P	4.17
L_P	3.44
W_F	0.525
L_F	4.18
W_g	12
L_g	3.9
W_1	2
L_1	1
W_2	1.6
L_2	0.8
W_3	0.25
L_3	0.25
W_a	14
W_b	19.72
W_c	24.82
L_{g1}	0.82
L_{g2}	0.52
L_{g3}	0.31
L_{g4}	0.2

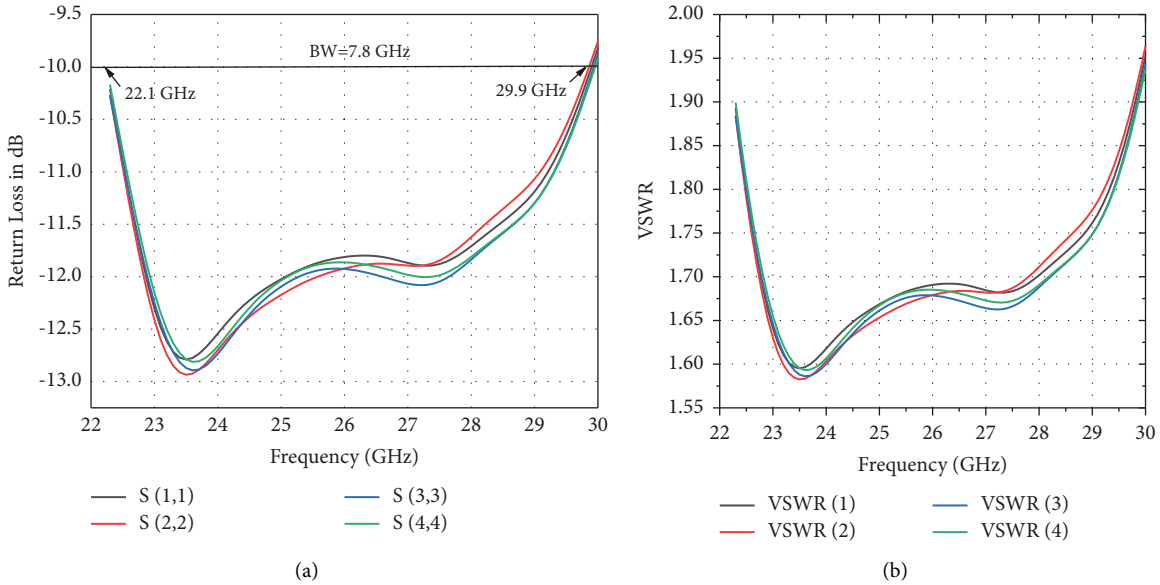

Figure 3: Continued.

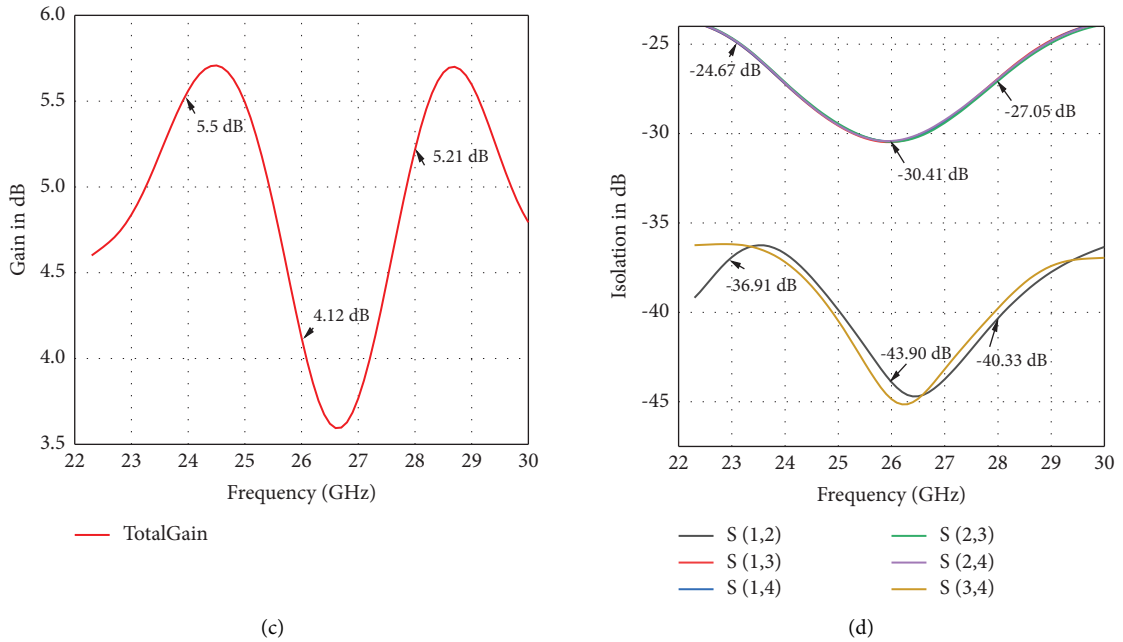

Figure 3: Simulation results of the self-isolated MIMO antenna design: (a) return loss, (b) VSWR, (c) gain, and (d) isolation.

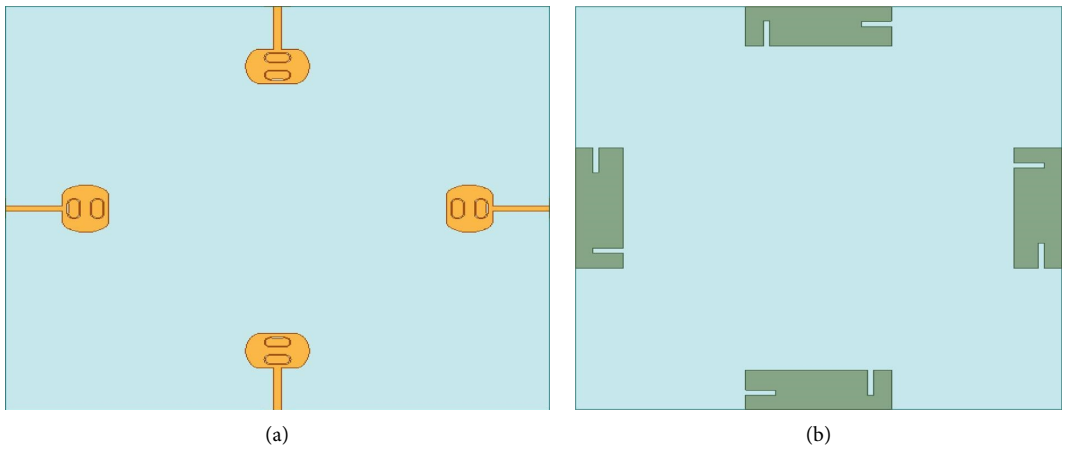

Figure 4: MIMO antenna with modified ground structure (MGS): (a) top view and (b) bottom view.

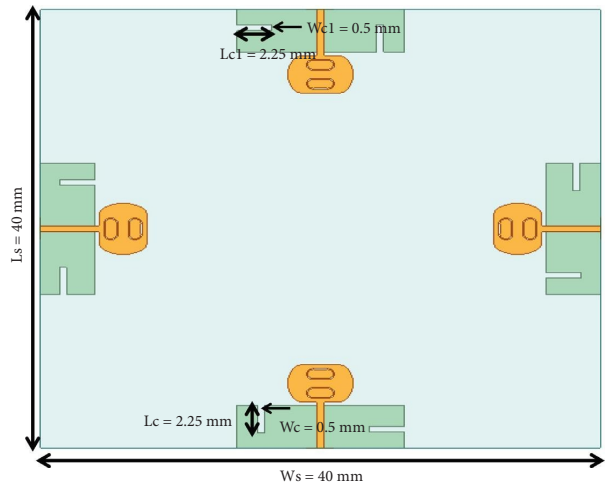

Figure 5: Dimensions of quad-port MIMO antenna with modified ground structure.

Table 3: The most suitable measurements for the suggested MGS antenna (in millimeters) are the optimal values.

Parameters	Values (mm)
W_s	40
L_s	40
H_S	0.8
W_c	0.5
L_c	2.25
W_{c1}	0.5
L_{c1}	2.25

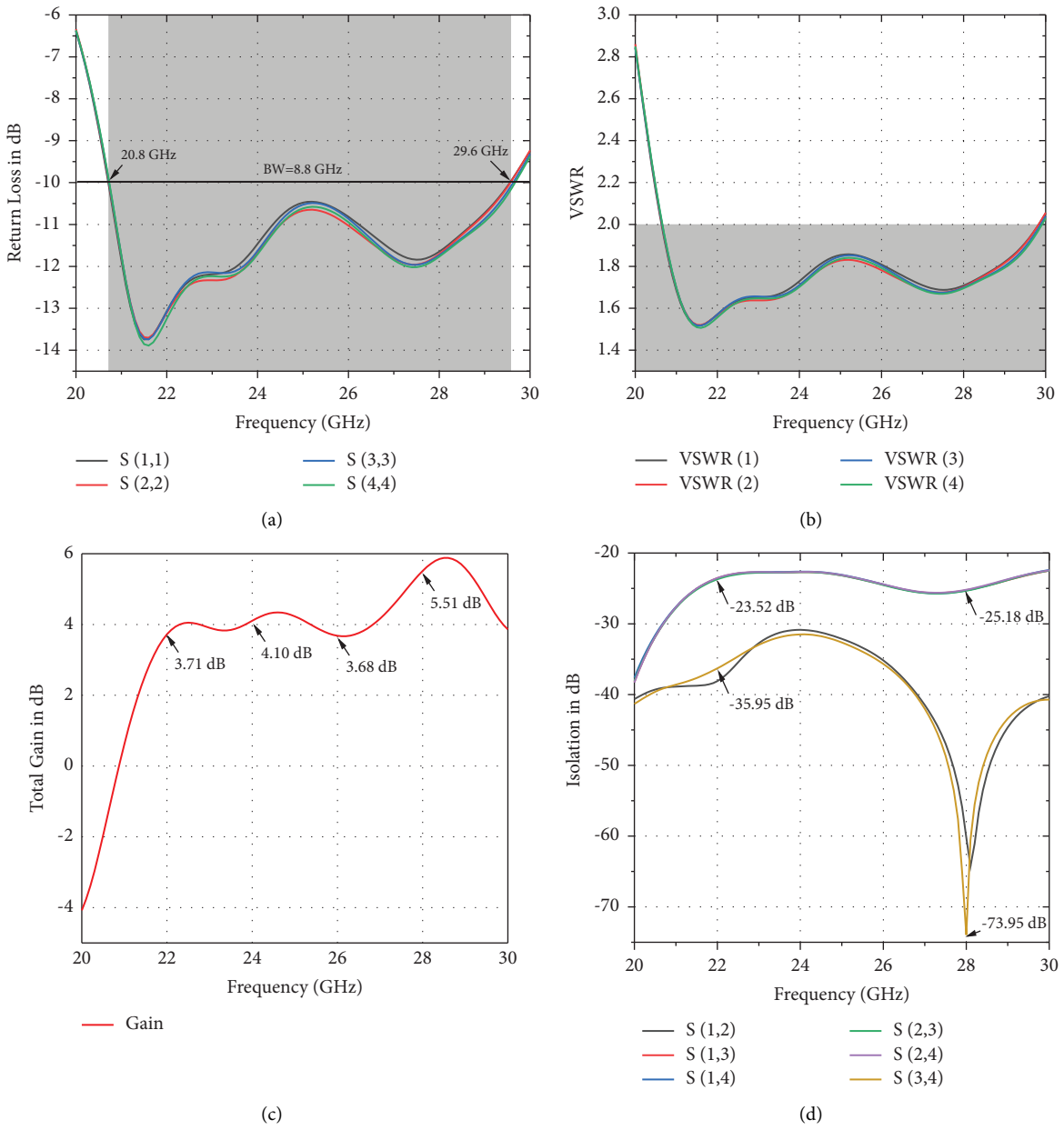

Figure 6: Simulation results of quad-port MIMO antenna design with modified ground structure (MGS): (a) return loss, (b) VSWR, (c) gain, and (d) isolation.

3.5. Hybrid Isolation Technique. In this technique, we combine the decoupling with defected ground structure (DGS), and as a result, the bandwidth is increased from the decoupling techniques from 6.6 GHz to 7.5 GHz and isolation is improved from −27 GHz to −28 GHz as well as the return loss is improved from −14 dB to −16 dB but

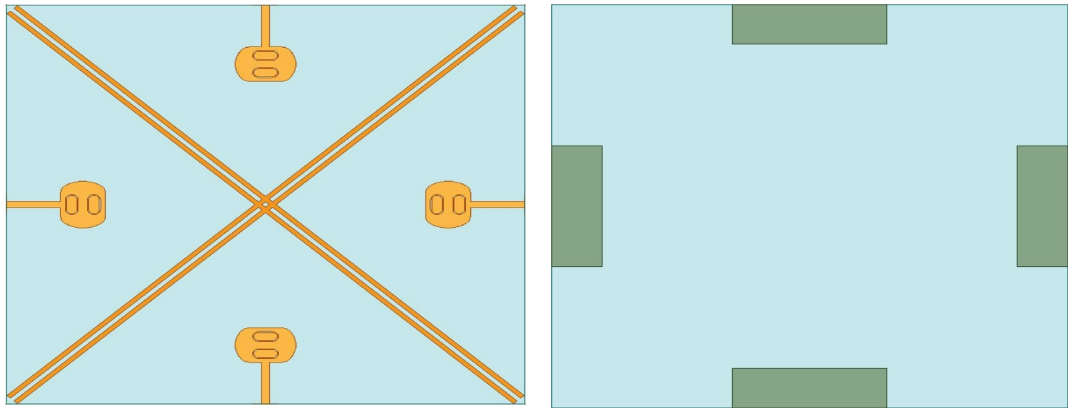

(a) (b)

Figure 7: MIMO antenna with decoupling structure: (a) top view and (b) bottom view.

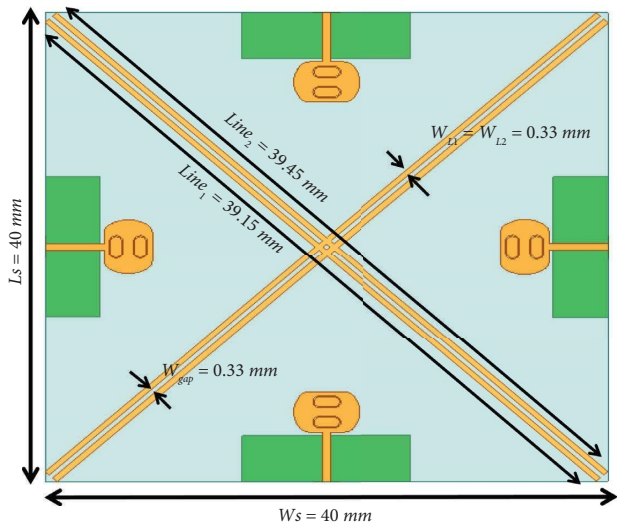

Figure 8: Dimensions of quad-port MIMO antenna with decoupling (X-shaped wall) structure.

Table 4: Optimal values of the proposed antenna dimensions for decoupling structure (all in mm).

Parameters	Values (mm)
W_S	40
L_S	40
H_S	0.8
Line_1	39.15
Line_2	39.45
W_{gap}	0.33
W_{L1}	0.33
W_{L2}	0.33

compromising with gain. Figure 13 shows the front and bottom views of the antenna, while Figure 14 shows the dimensions of the MIMO antenna with the hybrid technique. All dimensions are defined in mm values with respect to parameters in Table 6.

Figure 15 shows all simulated results of MIMO antenna with hybrid technique (combination of two isolation techniques such as decoupling structure with defected ground structure). Figure 15(a) shows return loss ($S11$), where the maximum return loss is −16.12 at 24.1 GHz frequency with ultra-wideband of 7.5 GHz. Figure 15(b) shows the VSWR which is less than 2, and the overall gain of the antenna within the entire band is maintained to 2 dB or greater than 4.15 dBi, and the isolation is improved from −23 dB to −28.84 dB. In this technique, the bandwidth and gain both are maintained but isolation is increased. So, for improving the isolation, the hybrid technique can be used.

The performance analysis of the MIMO antenna design with high isolation techniques for 5 G wireless systems yielded promising results. The proposed antenna design achieved high isolation between the antenna elements, ensuring minimal interference and improved overall system performance. Through extensive simulations and measurements, it was observed that the proposed antenna design achieved a high level of isolation, surpassing the requirements set by 5 G communication standards. This high isolation between the antenna elements led to enhanced system capacity and increased network efficiency. Furthermore, the MIMO antenna design exhibited excellent radiation pattern characteristics, maintaining a stable radiation pattern across different frequency bands. This ensured reliable and consistent signal transmission, minimizing signal degradation and maximizing coverage area. The results also demonstrated that the proposed antenna design contributed to significant improvements in bandwidth, gain, and isolation. The improved isolation and frequency bandwidth are crucial for 5 G wireless systems.

4. Measured Results for a Hybrid Model

The prototype antenna presented in this study was manufactured using the MITS-Eleven Lab printed circuit board machine, with a Roger RT/Duriod 5880 substrate. It consists of four antenna elements positioned on a compact substrate measuring 40 mm × 40 mm, as depicted in Figure 16. The

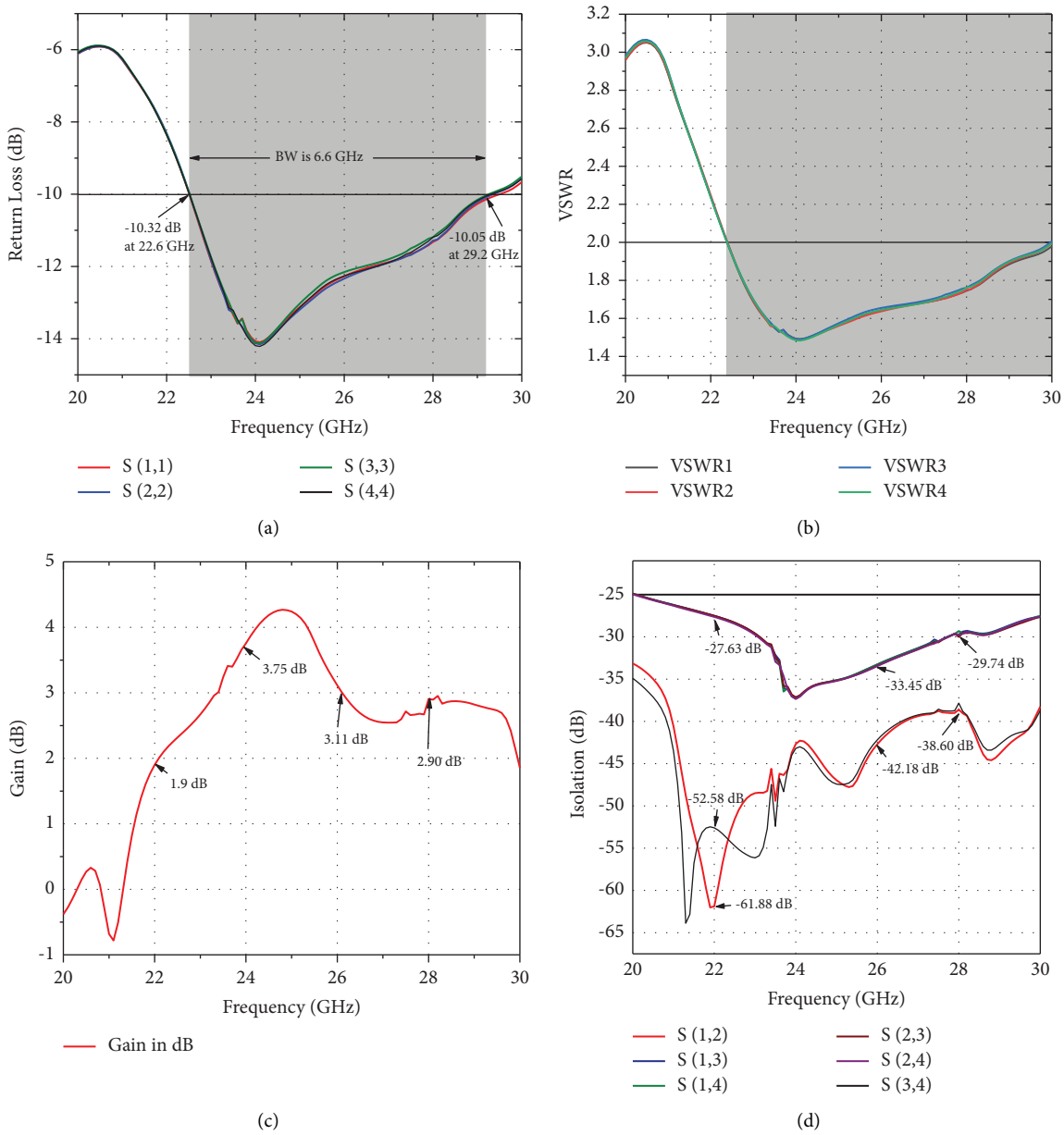

Figure 9: Simulation results of quad-port MIMO antenna design with introducing *X*-shaped decoupling structure: (a) return loss, (b) VSWR, (c) gain, and (d) isolation.

substrate was 0.8 mm thick, and its dielectric loss tangent value is 0.0009. To verify the accuracy of the simulated results, measurements were conducted on an Agilent N5230A vector network analyzer (VNA). Furthermore, radiation characteristics were evaluated within an anechoic chamber, as illustrated in Figure 17.

The measured results are compared with the simulation results to validate the antenna's performance. Figure 18 displays the S-parameter results, presenting a comparison between measured and simulated data. The measured return loss showed an impedance bandwidth ranging from 22 GHz to 29 GHz. This bandwidth meets the UWB requirement set by FCC. The measured and simulated outcomes from HFSS exhibited strong conformity.

In Figure 19, the measurement and simulation results of the isolation parameters are depicted. The analysis reveals that the values for *S*12 were consistently below −27 dB across the entire UWB range. This finding suggests that the proposed prototype exhibits minimal interference or coupling between its ports.

5. Diversity Parameters

Examining the MIMO antenna's effectiveness extends beyond merely scrutinizing return loss and isolation factors. To thoroughly gauge its performance, one must consider supplementary parameters such as ECC, diversity gain, TARC, and mean effective gain.

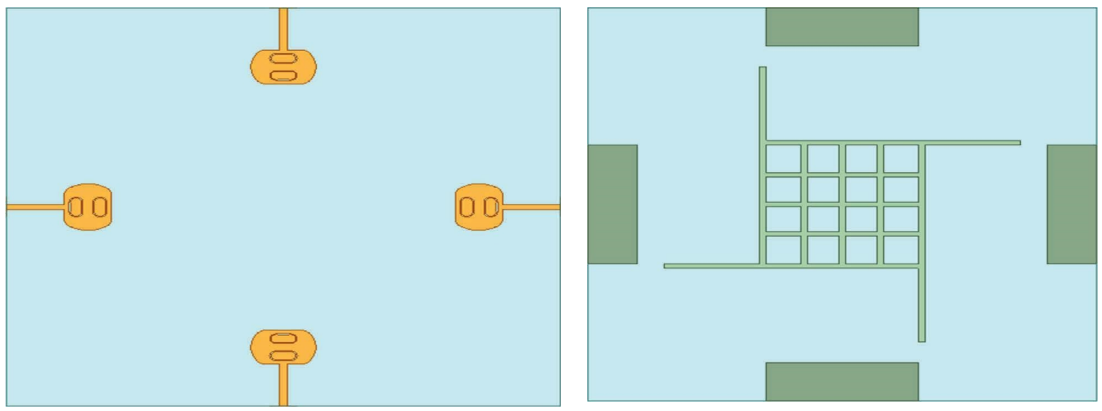

Figure 10: MIMO antenna that incorporates defected ground structure (DGS) technology: (a) top view and (b) bottom view.

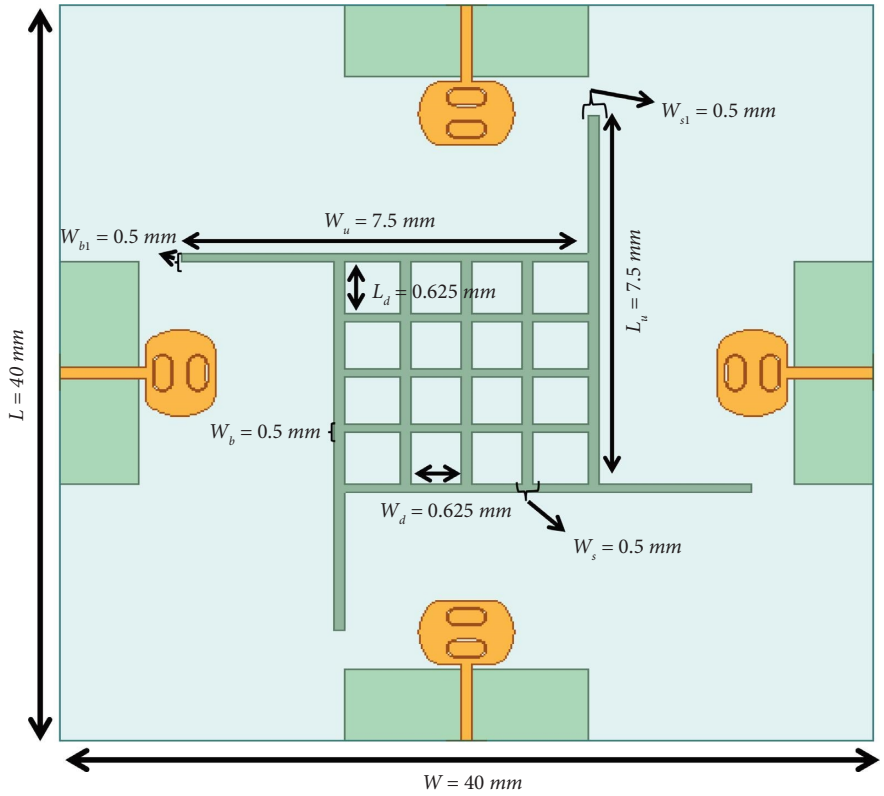

Figure 11: Dimensions of quad-port MIMO antenna with defected ground structure (DGS).

Table 5: The ideal values of the suggested antenna's dimensions for DGS (all in millimeters).

Parameters	Values (mm)
W	40
L	40
H_S	0.8
W_u	7.5
L_u	7.5
W_d	0.625
L_d	0.625
W_b	0.5
W_{b1}	0.5
W_s	0.5
W_{s1}	0.5

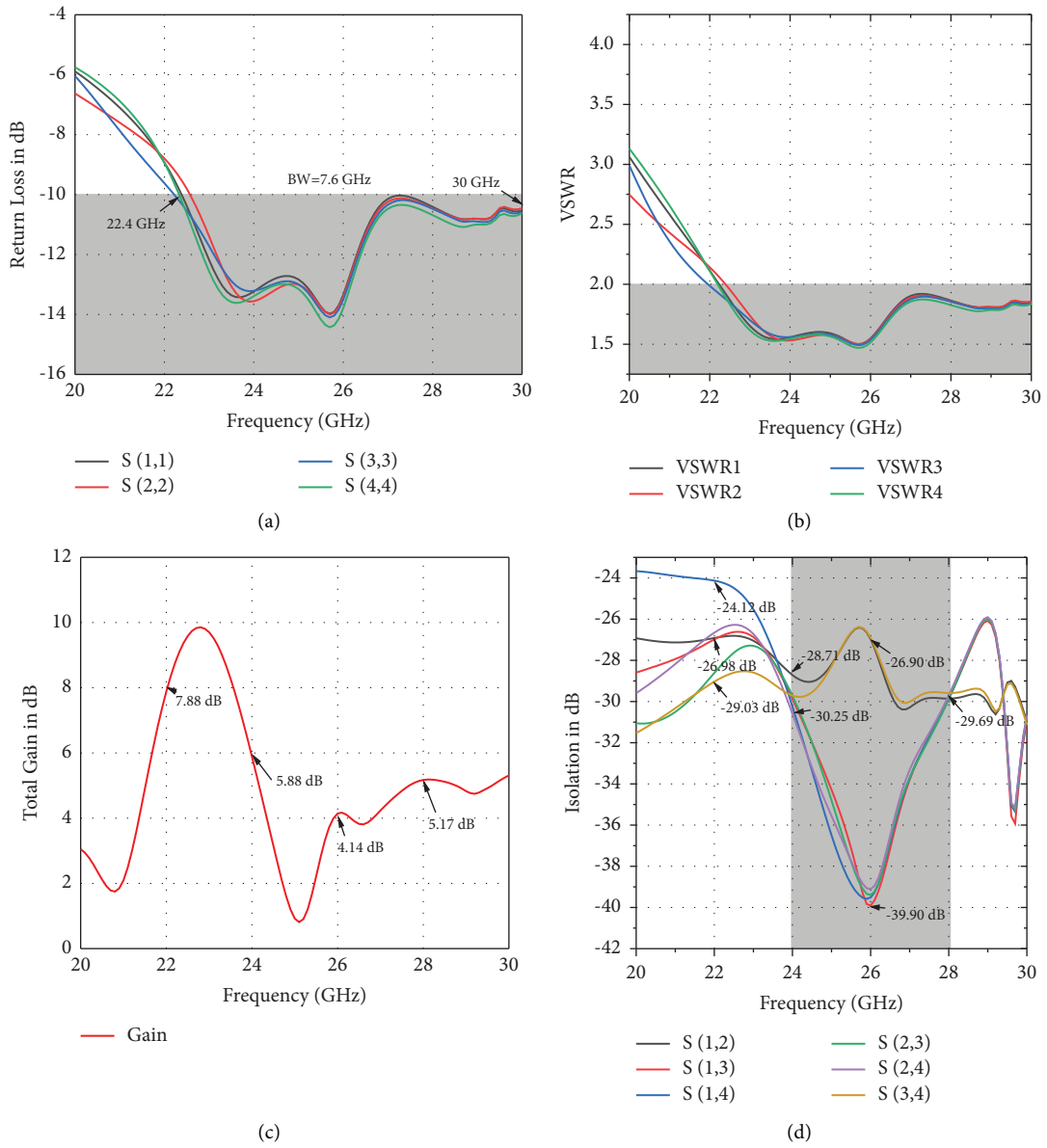

Figure 12: The results obtained from simulating the quad-port MIMO antenna design using defected ground structure (DGS): (a) return loss, (b) VSWR, (c) gain, and (d) isolation.

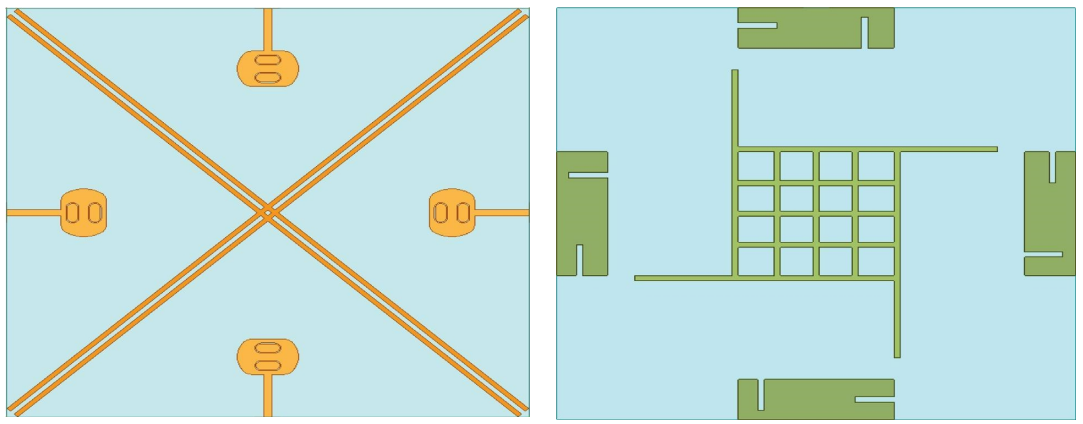

Figure 13: MIMO antenna with the hybrid technique: (a) top view and (b) bottom view.

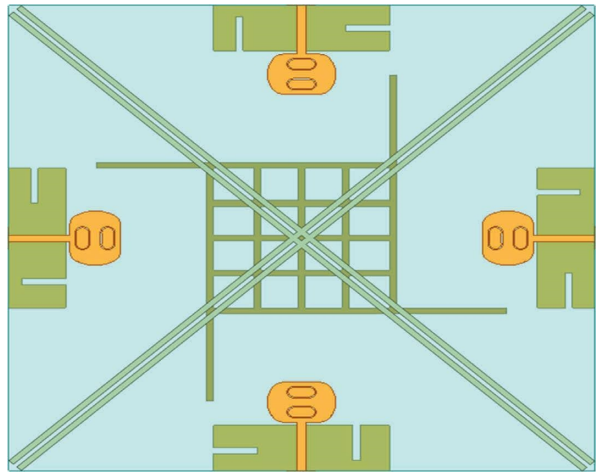

Figure 14: Dimensions of quad-port MIMO antenna with combination of decoupling and defected ground structure (DGS).

Table 6: Optimal values of the proposed antenna dimensions for DGS (all in mm).

Parameters	Values (mm)
W_u	7.5
L_u	7.5
W_d	0.625
L_d	0.625
W_b	0.5
W_{b1}	0.5
W_s	0.5
W_{s1}	0.5
Line_1	39.15
Line_2	39.45
W_{gap}	0.33
W_{L1}	0.33
W_{L2}	0.33

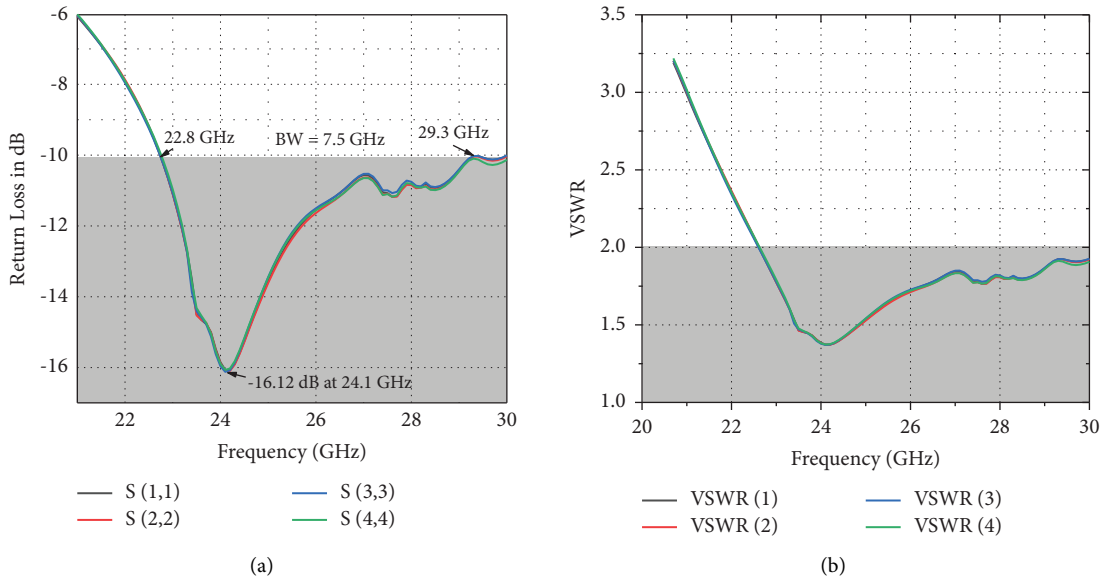

Figure 15: Continued.

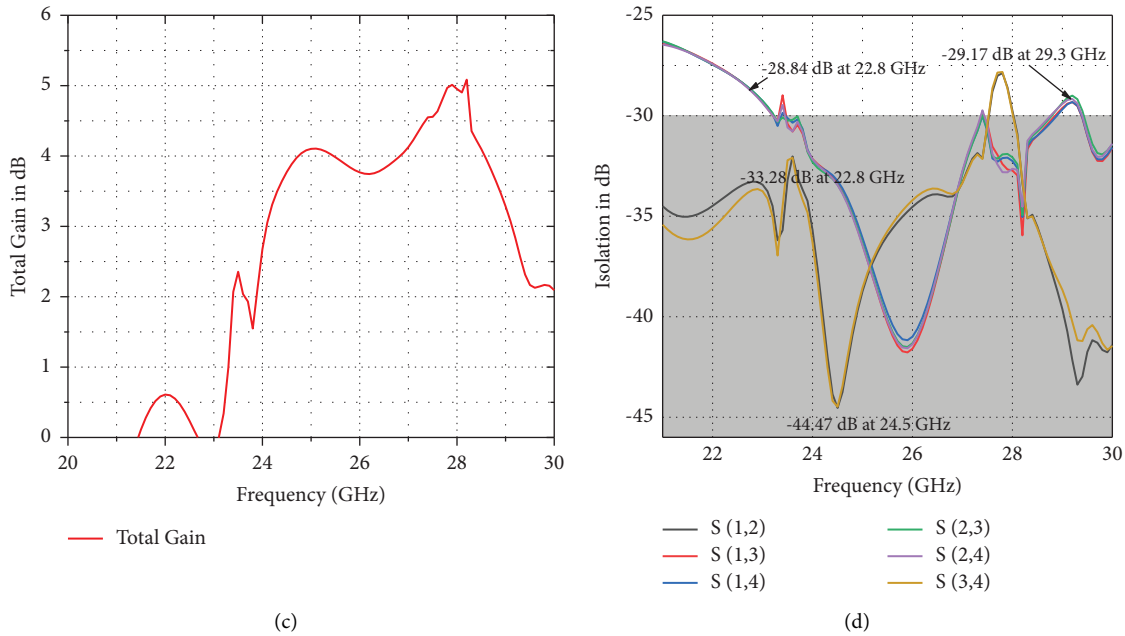

(c) (d)

FIGURE 15: Simulation results of quad-port MIMO antenna design with hybrid technique: (a) return loss, (b) VSWR, (c) gain, and (d) isolation.

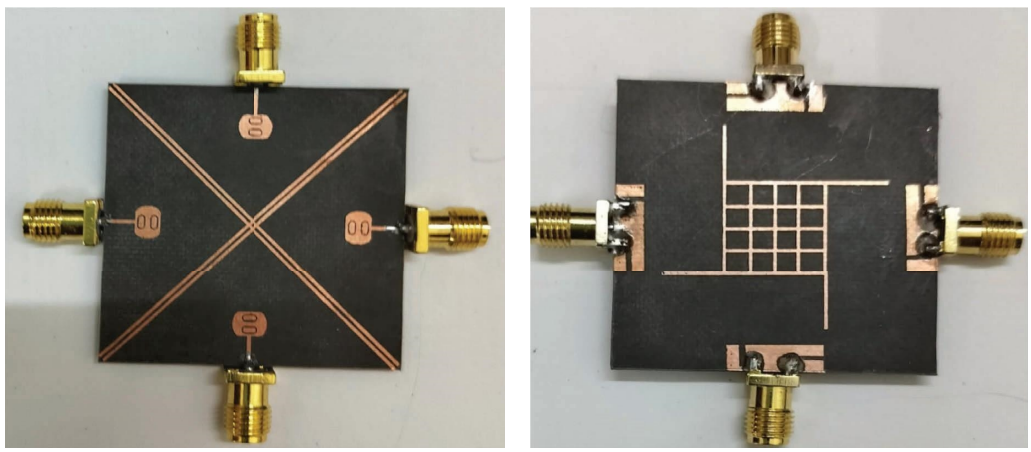

(a) (b)

FIGURE 16: Fabricated prototype. (a) Top view. (b) Bottom view.

5.1. Envelope Correlation Coefficient (ECC). The mutual coupling between antenna elements is significantly influenced by the diversity parameter, making it a crucial factor. The evaluation of ECC can be carried out in two ways: by analyzing the far-field radiation pattern and by assessing the *S*-parameter, and its calculation is given in the following equation:

$$\mathrm{ECC}(k,m) = \rho_e(k,m,N) = \frac{\left|\sum_{n=1}^{N} S_{k,n}^{*} S_{m,j}\right|^2}{\left|\prod_{l=k.m}\left(1 - \sum_{n=1}^{N} S_{l,n}^{*} S_{n,l}\right)\right|}, \tag{13}$$

where N = number of antenna elements and i and j are the port numbers.

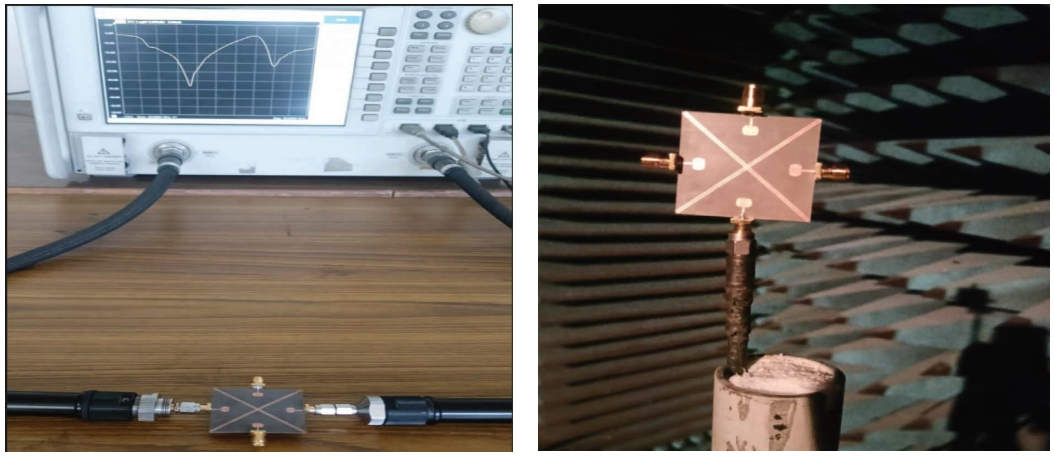

(a) (b)

Figure 17: Measurement setup with VNA (a) and anechoic chamber (b).

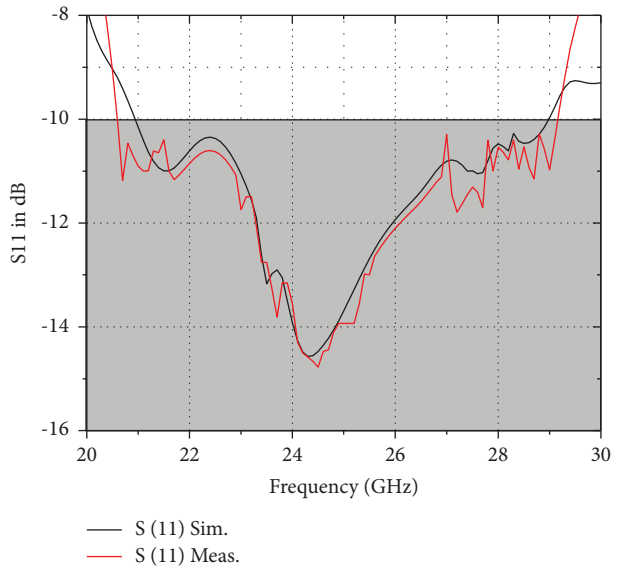

Figure 18: Simulated and measured $S11$ in dB.

By inserting $N = 4$ in equation (13), the ECC between antenna elements for a quad-port MIMO antenna may be calculated. For devices, the acceptable value of ECC should be less than 0.5.

$$\mathrm{ECC}_{12} = \rho_e(1,2,4) = \frac{\left|S_{11}^* S_{12} + S_{21}^* S_{22} + S_{13}^* S_{32} + S_{14}^* S_{42}\right|^2}{\left(1 - \left|S_{11}\right|^2 - \left|S_{21}\right|^2 - \left|S_{31}\right|^2 - \left|S_{41}\right|^2\right)\left(1 - \left|S_{12}\right|^2 - \left|S_{22}\right|^2 - \left|S_{32}\right|^2 - \left|S_{42}\right|^2\right)}, \tag{13a}$$

where ECC_{12} is the mutual coupling on port-1 due to port-2. Similarly, ECC_{13}, ECC_{14}, ECC_{23}, ECC_{24}, ...etc., can be evaluated from equation (13).

Figure 20 illustrates that the ECC value remains consistently below 0.005 across the entire operational range. The measured value is significantly lower than the practical value

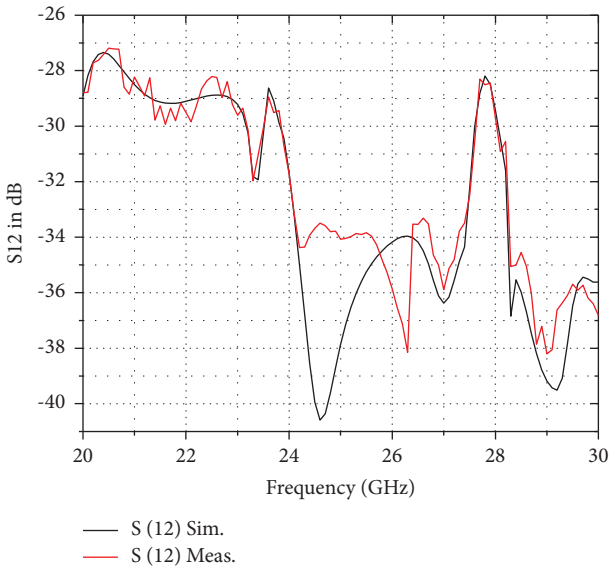

Figure 19: Simulated and measured $S12$ in dB.

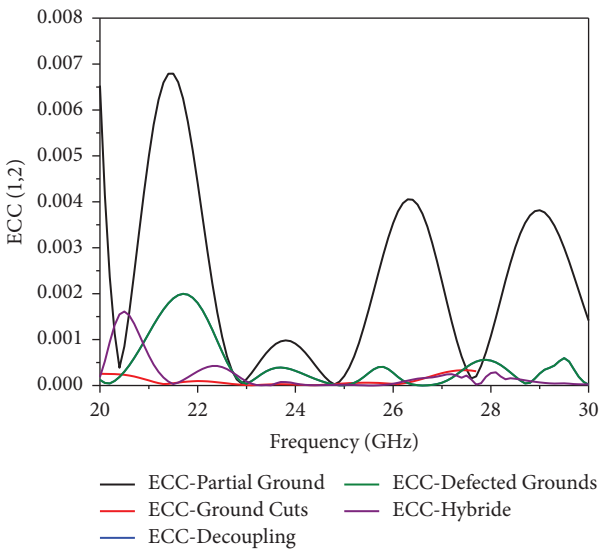

Figure 20: Simulated and measured ECC plots.

of 0.005 for all isolation techniques with in the entire frequency band of operation. Here, the hybrid model gives the better ECC value which is lower than 0.0025.

5.2. Diversity Gain (DG). A well-known measurement used to assess the effectiveness of diversity is the antenna diversity gain (DG). It can be described as the ratio of the system's single antenna's SNR to the increase in SNR of mixed signals from multiple antennas. For the MIMO antenna to function properly, the diversity gain, which can be calculated directly from the ECC value, should be closer to 10 dB. Diversity gain (DG) [36] evaluation of the proposed antenna can be done using the following formula:

$$\mathrm{DG}_{12} = 10\sqrt{1 - \left|\mathrm{ECC}_{12}\right|^2}. \tag{14}$$

Similarly, DG_{13}, DG_{14}, DG_{23}, DG_{24}, ...etc. can be evaluated from equation (14).

The MIMO antenna demonstrates remarkable performance with a diversity gain of 10 dB with all the models or (all isolation techniques). In Figure 21, it is evident that even when port 1 is active and the other port is inactive, the diversity gain consistently remains at 10 dB. This exceeds the widely accepted threshold of 9.5 dB, signifying excellent diversity performance. Furthermore, the value of 10 dB represents the optimal level of diversity gain, underscoring the exceptional capabilities of the prototype antenna in terms of diversity.

5.3. Total Active Reflection Coefficient (TARC). Operating bandwidth and efficiency in the MIMO system will be impacted when all antenna elements are active at once. As a result, S-parametric data are insufficient to determine how effective the antenna is, thus we used TARC, another crucial parameter, to assess the antenna's performance. The formula can be used to measure TARC [37, 38] is given as follows:

$$\mathrm{TARC} = \frac{\sqrt{\sum_{k=1}^{4}\left(\left|R_k\right|^2\right)}}{\sum_{k=1}^{4}\left(\left|I_k\right|^2\right)}, \tag{15}$$

where R_k is the reflected signal and I_k is the incident signal.

Assuming that all incoming signals at all ports have the same amplitude and phase (0° phase difference) in the suggested MIMO antenna, the equation for TARC is presented in Figure 22.

$$\mathrm{TARC} = \sqrt{\frac{\left|S_{11} + S_{12} + S_{13} + S_{14}\right|^2 + \left|S_{21} + S_{22} + S_{23} + S_{24}\right|^2 + \left|S_{31} + S_{32} + S_{33} + S_{34}\right|^2 + \left|S_{41} + S_{42} + S_{43} + S_{44}\right|^2}{4}}. \tag{16}$$

5.4. Channel Capacity Loss (CCL). The channel capacity loss refers to the maximum amount of data that can be reliably transmitted through a transmission channel. In MIMO systems, the accepted limit for practical purposes is usually below 0.4 bits per second per hertz across the entire frequency range used. The evaluation of CCL can be performed by the following steps [39]:

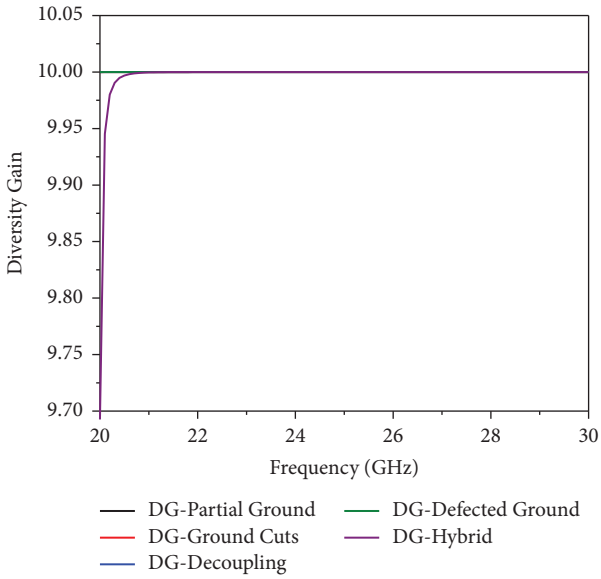

Figure 21: Simulated and measured DG plots.

$$C_{\text{Loss}} = -\log_2 \det\left(\varphi^R\right), \tag{17}$$

$$\varphi^R = \begin{bmatrix} \partial_{11} & \partial_{12} & \partial_{13} & \partial_{14} \\ \partial_{21} & \partial_{22} & \partial_{23} & \partial_{24} \\ \partial_{31} & \partial_{32} & \partial_{33} & \partial_{34} \\ \partial_{41} & \partial_{42} & \partial_{43} & \partial_{44} \end{bmatrix},$$
$$\partial_{ii} = \left(1 - \left|S_{ii}\right|^2 - \left|S_{ij}\right|^2\right), \tag{17a}$$
$$\partial_{ij} = -\left(S_{ii}^* S_{ij} + S_{ji}^* S_{ij}\right) \text{for } i, \quad j = 1, 2, 3, \text{and } 4.$$

The correlation matrix for the receiving antenna is denoted as φ^R. In the case of an N port MIMO system, this matrix can be calculated using the following method.

Figures 22 and 23 show the measured TARC and channel capacity loss (CCL), demonstrating that the channel capacity loss remains below 0.4 bits/s/Hz except the ground cut model has 0.6 bits/s/Hz and the TARC remains below −10 dB across the entire frequency range.

The MIMO antenna suggested in this research displays distinctive characteristics, as indicated in Tables 1 and 7. First, it provides extensive coverage for high-frequency 5 G wireless applications, surpassing the range of reference [10, 17–29]. Second, its isolation surpasses that of the antennas mentioned in [10, 17–29], maintaining a level above −27 dB across the entire operating band. Additionally, the proposed antenna has smaller dimensions compared to [10, 19–22, 26, 29]. Moreover, it exhibits a wide range of impedance bandwidth, surpassing all antennas documented in [10, 17–29]. Furthermore, the suggested antenna is not dependent on a three-dimensional structure, making it simple to fabricate and less complex.

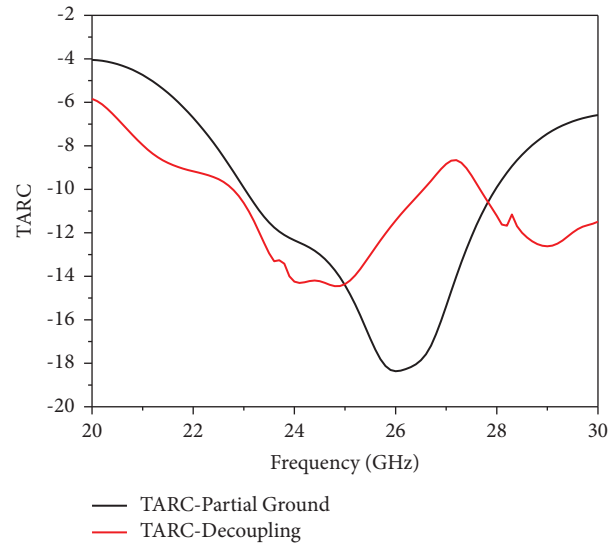

Figure 22: Measured TARC versus frequency plot.

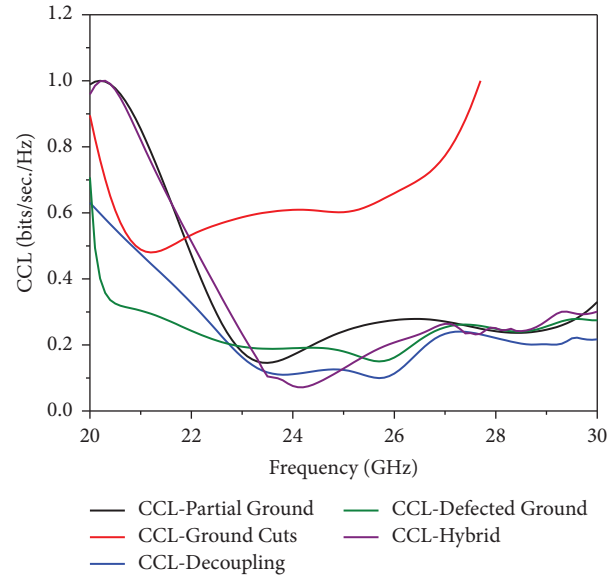

Figure 23: Measured CCL versus frequency plot.

Lastly, the proposed MIMO antenna provides complete coverage of the K-band within a single ultrawide band.

Here, Table 8 compares all designed antenna simulated results. The size of the antenna is $40 \times 40 \times 0.8\,\text{mm}^3$ and is placed on the Rogers RT/Duroid 5880 substrate. It seems that the hybrid model improved the isolation while maintaining the other parameters. . Its ability to achieve high isolation, maintain stable radiation patterns, and enhance signal quality metrics makes it a valuable choice for future 5 G technology.

Table 7: Comparison of simulated results for isolation techniques.

S. No	Isolation technique	Frequency range (GHz)	Band width (BW GHz)	Return loss (S11-dB)	Average gain (dBi)	Isolation (dB)	ECC	DG	CCL
1	Self-isolation	22.1 to 29.9	7.8	−13	>5.85	>−23	<0.0067	9.98	<0.4
2	Modified ground structure (MGS)	20.8 to 29.6	8.8	−14	>5.86	>−23.52	<0.002	9.99	>0.6
3	Defected ground structure (DGS)	22.4 to 30	7.6	−14.73	>6.29	>24	<<0.002	9.99	<0.5
4	Decoupling (*X*-shaped wall) structure	22.6 to 29.2	6.6	−14.3	>4.15	>−27.63	<<0.002	9.99	<0.4
5	Hybrid model	22.8 to 29.3	7.5	−16.12	>4.72	>−28.84	<<0.002	9.99	<0.4

Table 8: The performance comparison in relation to prior studies published literature.

Ref. no./year	Size of antenna	No. of elements	Substrate	BW (GHz)	Isolation (dB)	Gain (dBi)	ECC	DG	CCL	Radiation efficiency (%)
Reference [40]/2017	40 × 40 × 1.6	4	FR4	3.1 to 11	<−20	3	<0.004	—	—	—
Reference [41]/2019	40 × 43 × 1	4	FR4	3.1 to 10.6	<−20	4	<0.2	—	0.3	92
Reference [42]/2019	40 × 40 × 1.6	4	FR4	3 to 12	<−17	2.9	<0.06	—	—	—
Reference [43]/2021	40 × 40 × 1.6	4	FR4	11 to 13	<−15	6	<0.4	—	<0.4	—
Reference [44]/2021	40 × 40 × 1.6	4	FR4	3 to 3.5	<−15	3	<0.4	>9.95	—	89
Reference [45]/2021	40 × 40 × 1.5	4	FR4 laminate	3.1 to 10.6	<−16	2.9	<0.13	—	0.25	90
Reference [46]/2022	40 × 40 × 1.6	4	FR4	3.1 to 13.75	<−18	8	<0.012	—	<0.3	>89
Reference [47]/2022	28 × 40 × 1.6	4	FR4	3.1 to 13.75	<−25	8.1	<0.004	>9.92	<0.39	>90
Reference [48]/2023	40 × 40 × 1.6	4	FR4	2.8 to 11.4	<−26	8.5	<0.001	>9.99	0.28	90
Prop. work (hybrid model)	40 × 40 × 0.8	4	Roger RT/Duriod 5880	22.8 to 29.3	<−28.84	6.87	<0.005	10.0	0.4	>97

6. Conclusion

When designing a MIMO antenna with various isolation techniques, it is crucial to thoroughly analyze the antenna type, design properties, and the desired level of isolation. This careful consideration is essential for optimizing the antenna's overall performance. Each type of isolation technique offers unique features that are suited to certain types of wireless communication systems, ranging from low-cost conventional methods to more complex signal cancellation techniques. As a result, the selection of the most suitable isolation technique for any given MIMO antenna design depends on the individual goals and requirements of the system. The suggested MIMO antenna comprising four elements, with decoupling structure (introducing the *X*-shaped wall between the radiating elements), is an effective solution for 5 G communications. Operating at a frequency range between 22.5 GHz and 29.1 GHz, the antenna offers an isolation level of 27.63 dB and a gain enhancement of 6.39 dBi, while the hybrid technique improved the isolation till 28.84 dB as well as improved the bandwidth from 6.6 GHz to 7.5 GHz with maintained gain. HFSS software simulations demonstrate excellent agreement between the expected results and the parameters observed, including return loss, voltage standing wave ratio (VSWR), isolation level, and peak gain, throughout the operating band. These outcomes affirm the antenna's dependable suitability for 5 G communications. Here, the hybrid technique is the best suitable isolation technique for the proposed MIMO antenna design.

7. Future Scope

It is a common belief that every technology will eventually reach a point of saturation, either due to demand or the emergence of a more efficient alternative. With this in mind, we can propose certain measures that can be adopted to meet future demand and enhance the existing work. The antenna will be manufactured and all its characteristics will be assessed within an anechoic chamber. After integration into a device such as a mobile phone, laptop, or other wireless portable gadgets, the functionality of the designed antenna can be analyzed. One possible way to decrease the antenna size is to incorporate metamaterial, metasurface, or a blend of these elements, to utilize any other appropriate technique.

Data Availability

The data supporting the findings of this research are available on request from the first author upon reasonable request.

Conflicts of Interest

The authors declare that there are no conflicts of interest.

Authors' Contributions

Suverna Sengar conceptualized the study, proposed the methodology, prepared the original draft, and performed fabrication and testing. Praveen Kumar Malik supervised the study, formally analyzed the study, investigated the study, and collected the data. Puneet Chandra Srivastava performed the software analysis, validated the study, and visualized the study. Kiran Srivastava gathered the resources, collected the data, and analyzed the study. Anita Gehlot supervised the study and reviewed and edited the manuscript.

References

[1] T. Rappaport, S. Sun, R. Mayzus et al., "Millimeter wave mobile communications for 5G cellular: it will work!" *IEEE Access*, vol. 1, pp. 335–349, 2013.

[2] J. Powell and A. Chandrakasan, "Differential and single ended elliptical antennas for 3.1–10.6 GHz ultrawideband communication," in *Proceedings of the Antennas and Propagation Society International Symposium*, pp. 2935–2938, Sendai, Japan, June 2004.

[3] A. S. Abd El-Hameed, M. G. Wahab, N. A. Elshafey, and M. S. Elpeltagy, "Quad-port UWB MIMO antenna based on LPF with vast rejection band," *AEU-International Journal of Electronics and Communications*, vol. 134, Article ID 153712, 2021.

[4] H. Manoharan, S. Selvarajan, A. Yafoz et al., "Deep conviction systems for biomedical applications using intuiting procedures with cross point approach," *Frontiers in Public Health*, vol. 10, Article ID 909628, 2022.

[5] A. Iqbal, A. Smida, A. J. Alazemi, M. I. Waly, N. Khaddaj Mallat, and S. Kim, "Wideband circularly polarized MIMO antenna for high data wearable biotelemetric devices," *IEEE Access*, vol. 8, pp. 17935–17944, 2020.

[6] T. Kaiser, Z. Feng, and E. Dimitrov, "An overview of ultra-wide-band systems with MIMO," *Proceedings of the IEEE*, vol. 97, no. 2, pp. 285–312, 2009.

[7] A. A. Ibrahim, M. A. Abdalla, A. B. Abdel-Rahman, and H. F. Hamed, "Compact MIMO antenna with optimized mutual coupling reduction using DGS," *International Journal of Microwave and Wireless Technologies*, vol. 6, no. 2, pp. 173–180, 2014.

[8] A. Toktas and A. Akdagli, "Compact multiple-input multiple-output antenna with low correlation for ultra-wide-band applications," *IET Microwaves, Antennas and Propagation*, vol. 9, no. 8, pp. 822–829, 2015.

[9] S. Zhang and G. F. Pedersen, "Mutual coupling reduction for UWB MIMO antennas with a wideband neutralization line," *IEEE Antennas and Wireless Propagation Letters*, vol. 15, pp. 166–169, 2016.

[10] A. Iqbal, O. A. Saraereh, A. W. Ahmad, and S. Bashir, "'Mutual coupling reduction using F-Shaped stubs in UWB-MIMO antenna," *IEEE Access*, vol. 6, pp. 2755–2759, 2018.

[11] H. Wang, Z. Zhang, and Z. Feng, "Dual-port planar MIMO antenna with ultra-high isolation and orthogonal radiation patterns," *Electronics Letters*, vol. 51, no. 1, pp. 7-8, 2015.

[12] M. E. Munir, S. H. Kiani, H. S. Savci et al., "A four element mm-wave MIMO antenna system with wide-band and high isolation characteristics for 5G applications," *Micromachines*, vol. 14, no. 4, p. 776, 2023.

[13] J. Kulkarni, A. Desai, and C.-Y. Sim, "Two port CPW-fed MIMO antenna with wide bandwidth and high isolation for future wireless applications," *International Journal of RF and Microwave Computer-Aided Engineering*, vol. 31, no. 8, 2021.

[14] S. Senger and P. K. Malik, "A comprehensive survey of massive-MIMO based on 5G antennas," *International Journal of RF and Microwave Computer-Aided Engineering*, vol. 32, no. 12, 2022.

[15] K. C. Ravi and J. Kumar, "Miniaturized parasitic loaded high-isolation MIMO antenna for 5G applications," *Sensors*, vol. 22, no. 19, p. 7283, 2022.

[16] P. B. Nikam, J. Kumar, V. Sivanagaraju, and A. Baidya, "Dual-band reconfigurable EBG loaded circular patch MIMO antenna using defected ground structure (DGS) and PIN diode integrated branch-lines (BLs)," *Measurement*, vol. 195, Article ID 111127, 2022.

[17] E. Al Abbas, M. Ikram, A. T. Mobashsher, and A. Abbosh, "MIMO antenna system for multi band millimeter-wave 5G and wideband 4G mobile communications," *IEEE Access*, vol. 7, pp. 181916–181923, 2019.

[18] L. Chang and H. Wang, "Miniaturized wideband four-antenna module based on dual-mode PIFA for 5G 4 × 4 MIMO applications," *IEEE Transactions on Antennas and Propagation*, vol. 69, no. 9, pp. 5297–5304, 2021.

[19] H. Sakli, C. Abdelhamid, C. Essid, and N. Sakli, "Metamaterial-based antenna performance enhancement for MIMO system applications," *IEEE Access*, vol. 9, pp. 38546–38556, 2021.

[20] W. Wu, B. Yuan, and A. Wu, "A quad-element UWB-MIMO antenna with band-notch and reduced mutual coupling based on EBG structures," *International Journal of Antennas and Propagation*, vol. 2018, Article ID 8490740, 10 pages, 2018.

[21] V. S. D. Rekha, P. Pardhasaradhi, B. T. P. Madhav, and Y. U. Devi, "Dual band notched orthogonal 4-element MIMO antenna with isolation for UWB applications," *IEEE Access*, vol. 8, pp. 145871–145880, 2020.

[22] A. Ibrahim and W. Ali, "High isolation 4-element ACS-fed MIMO antenna with band notched feature for UWB communications," *International Journal of Microwave and Wireless Technologies*, vol. 14, no. 1, pp. 54–64, 2022.

[23] R. Mark, N. Rajak, K. Mandal, and S. Das, "Metamaterial based superstrate towards the isolation and gain enhancement of MIMO antenna for WLAN application," *AEU-International Journal of Electronics and Communications*, vol. 100, pp. 144–152, 2019.

[24] A. A. Ibrahim, W. A. E. Ali, M. Alathbah, and A. R. Sabek, "Four-port 38 GHz MIMO antenna with high gain and isolation for 5G wireless networks," *Sensors*, vol. 23, no. 7, p. 3557, 2023.

[25] A. Desai, C. D. Bui, J. Patel, T. Upadhyaya, G. Byun, and T. K. Nguyen, "Compact wideband four element optically transparent MIMO antenna for mm-wave 5G applications," *IEEE Access*, vol. 8, pp. 194206–194217, 2020.

[26] D. A. Sehrai, M. Abdullah, A. Altaf et al., "A novel high gain wideband MIMO antenna for 5G millimeter wave applications," *Electronics*, vol. 9, no. 6, p. 1031, 2020.

[27] M. Khalid, S. Iffat Naqvi, N. Hussain et al., "4-Port MIMO antenna with defected ground structure for 5G millimeter wave applications," *Electronics*, vol. 9, no. 1, p. 71, 2020.

[28] B. Yang, Z. Yu, Y. Dong, J. Zhou, and W. Hong, "Compact tapered slot antenna array for 5G millimeter-wave massive MIMO systems," *IEEE Transactions on Antennas and Propagation*, vol. 65, no. 12, pp. 6721–6727, 2017.

[29] N. Yoon and C. Seo, "A 28-GHz wideband 2×2 U-slot patch array antenna," *Journal of electromagnetic engineering and science*, vol. 17, no. 3, pp. 133–137, 2017.

[30] T. Shabbir, R. Saleem, A. Akram, and M. F. Shafique, "UWB-MIMO quadruple with FSS-inspired decoupling structures and defected grounds," *Applied computational electromagnetic*, vol. 30, no. 2, pp. 184–190, 2015.

[31] N. K. Kiem, H. N. Phuong, Q. N. Hieu, and D. N. Chien, "A compact printed 4×4 MIMO-UWB antenna with WLAN band rejection," in *Proceedings of the Antennas and Propagation Society International Symposium (APSURSI)*, pp. 2245-2246, Orlando, FL, USA, July 2013.

[32] L. Si, H. Jiang, X. Lv, and J. Ding, "Broadband extremely close-spaced 5G MIMO antenna with mutual coupling reduction using metamaterial-inspired superstrate," *Optics Express*, vol. 27, no. 3, pp. 3472–3482, 2019.

[33] A. Wu, Y. Tao, P. Zhang, Z. Zhang, and Z. Fang, "A compact high-isolation four-element MIMO antenna with asymptote-shaped structure," *Sensors*, vol. 23, no. 5, p. 2484, 2023.

[34] B. BharathiDevi and J. Kumar, "Small frequency range discrete bandwidth tunable multiband MIMO antenna forradio/LTE/ISM-2.4 GHz band applications," *AEU-International Journal of Electronics and Communications*, vol. 144, Article ID 154060, 2022.

[35] S. Roshani and H. Shahveisi, "Mutual coupling reduction in microstrip patch antenna arrays using simple microstrip resonator," *Wireless Personal Communications*, vol. 126, no. 2, pp. 1665–1677, 2022.

[36] K. V. Babu, S. Das, S. S. Ali, M. El Ghzaoui, B. T. P. Madhav, and S. K. Patel, "Broadband sub-6 GHz flower-shaped MIMO antenna with high isolation using theory of characteristic mode analysis (TCMA) for 5G NR bands and WLAN applications," *International Journal of Communication Systems*, vol. 36, no. 6, 2023.

[37] N. E. Nasri, S. Das, M. El Ghzaoui, B. T. P. Madhav, S. Vara Kumari, and M. Fattah, "A compact wideband (22–44GHz) printed 2 × 4 MIMO array antenna with high gain for 26/28/38GHz millimeter-wave 5G applications," *Journal of Circuits, Systems, and Computers*, Article ID 2350300, 2023.

[38] B. Aghoutane, S. Das, M. El Ghzaoui, B. Madhav, and H. El Faylali, "A novel dual band high gain 4-port millimeter wave MIMO antenna array for 28/37 GHz 5G applications," *AEU-International Journal of Electronics and Communications*, vol. 145, Article ID 154071, 2022.

[39] P. Tiwari, V. Gahlaut, M. Kaushik et al., "Enhancing performance of millimeter wave MIMO antenna with a decoupling and common defected ground approach," *Technologies*, vol. 11, no. 5, p. 142, 2023.

[40] W. A. E. Ali and A. A. Ibrahim, "A compact double-sided MIMO antenna with an improved isolation for UWB applications," *AEU-International Journal of Electronics and Communications*, vol. 82, pp. 7–13, 2017.

[41] F. Amin, R. Saleem, T. Shabbir, S. Rehman, M. Bilal, and M. F. Shafique, "A compact quad-element UWB-MIMO antenna system with parasitic decoupling mechanism," *Applied Sciences*, vol. 9, no. 11, p. 2371, 2019.

[42] S. Rajkumar, A. Anto Amala, and K. T. Selvan, "Isolation improvement of UWB MIMO antenna utilising molecule fractal structure," *Electronics Letters*, vol. 55, no. 10, pp. 576–579, 2019.

[43] A. A. Khan, S. A. Naqvi, M. S. Khan, and B. Ijaz, "Quad port miniaturized MIMO antenna for UWB 11 GHz and 13 GHz frequency bands," *AEU-International Journal of Electronics and Communications*, vol. 131, Article ID 153618, 2021.

[44] D. K. Raheja, B. K. Kanaujia, and S. Kumar, "Compact four-port MIMO antenna on slottededge substrate with dual-band rejection characteristics," *International Journal of RF and Microwave Computer-Aided Engineering*, vol. 29, no. 7, 2019.

[45] D. Singh, A. A. Khan, S. A. Naqvi et al., "Inverted-c ground MIMO antenna for compact UWB applications," *Journal of Electromagnetic Waves and Applications*, vol. 35, no. 15, pp. 2078–2091, 2021.

[46] A. C. Suresh and T. S. Reddy, "A flower shaped miniaturized 4×4 MIMO antenna for UWB applications using

characteristic mode analysis," *Progress in Electromagnetics Research C*, vol. 119, pp. 219–233, 2022.

[47] A. C. Suresh, T. S. Reddy, B. T. P. Madhav et al., "Investigations on stub-based UWB-MIMO antennas to enhance isolation using characteristic mode analysis," *Micromachines*, vol. 13, no. 12, p. 2088, 2022.

[48] A. C. Suresh, T. S. Reddy, and S. V. Svuce, "Experimental investigation of novel frock-shaped miniaturized 4×4 UWB MIMO antenna using characteristic mode analysis," *Progress in Electromagnetics Research B*, vol. 101, pp. 45–61, 2023.